Perturbation growth in terms of baroclinic alignment properties

By G. RIVIÈRE[1]*, B. L. HUA[2] and P. KLEIN[2]

SUMMARY

Mechanisms leading to perturbation growth in complex time-dependent quasi-geostrophic (QG) flows are addressed in this paper. The dynamics of small three-dimensional (3D) perturbations are studied for the complete set of the linearized local QG equations. An analytical diagnostic of these equations shows that, at each spatial location, the preferred 3D structures of the perturbations are related to the eigenvector directions of a matrix, denoted $\bar{\mathbf{A}}$, which is the 3D generalization of the basic-state strain-rate tensor. The matrix $\bar{\mathbf{A}}$ has a degenerate form and depends on both the horizontal deformation and the vertical shear of the unperturbed reference flow. By using a nonlinear Monte-Carlo technique, the 3D structures related to $\bar{\mathbf{A}}$'s eigenvectors are shown to be the most probable ones for perturbation growth. We also provide simple analytical expressions for quantifying the barotropic and baroclinic energy extraction from the reference flow by the perturbations. In particular, our analytical expression for baroclinic energy extraction is found to be more relevant than the Eady index widely used in the literature. An interesting outcome of the Monte-Carlo simulations is that the maxima of the total-energy error field are found to be localized in regions where the norm of $\bar{\mathbf{A}}$ is large.

KEYWORDS: Alignment dynamics   Local baroclinic instability   Total-energy growth

1. INTRODUCTION

The understanding of the dynamics of perturbation growth in spatially and temporally complex flows is crucial to making progress in a variety of atmospheric and oceanic problems. Mechanisms underlying forecast errors in meteorology and oceanography due to uncertain initial conditions (the so-called initial-error growth) can be viewed as the growth of small perturbations that extract energy from a reference flow. The study of perturbation growth not only permits us to address the predictability problem but also is useful for exploring dynamical aspects of various phenomena with different space- and time-scales such as cyclogenesis processes and storm-track behaviours.

Two areas of research can be distinguished in the study of perturbation dynamics. Historically, since the works of Eady (1949) and Charney (1947) on normal modes in steady parallel flows, there has been an intensive period of research to quantify analytically the growth of disturbances for prescribed basic states. Progress originated from the consideration of increasingly complex basic states and from an examination of the whole set of perturbations, i.e. both modal and nonmodal perturbations (e.g. Farrell 1982, 1989). However, there is usually a wide gap between basic states that are amenable to analytical calculations and realistic flows. The other area of research involves numerical models that simulate more accurately the behaviour of realistic flows and consists of perturbing the basic state with different types of dynamically relevant perturbations: singular vectors, normal modes, adjoint modes, Lyapunov vectors and bred modes (see e.g. Buizza and Palmer 1995; Szunyogh *et al.* 1997; Frederiksen 2000). All the results developed in this second type of study are numerical and not analytical. They also have the disadvantage of quantifying the growth of perturbations globally for a chosen area and not locally in physical space. Our approach in the present paper differs from these two types of study since the goal is to develop analytical and local diagnostics

* Corresponding author, present affiliation: Geophysical Fluid Dynamics Laboratory, Forrestal Campus, PO Box 308, Princeton NJ 08542, USA. e-mail: griviere@princeton.edu

to describe the statistical characteristics of the growth of small perturbations for any time-dependent and spatially complex quasi-geostrophic (QG) flow. More specifically, we focus on the alignment properties of the perturbations, i.e. on the orientation of the perturbation stream-function gradient, whose role is crucial in determining whether the perturbation is effective for extracting energy from the basic flow.

A first approach by considering only barotropic processes (Rivière *et al.* 2003, referred to as RHK hereafter) leads to the following result: the most probable horizontal structures of the perturbations that have evolved for a finite time (corresponding approximately to 5 straining time-scales of the reference flow) can be analytically diagnosed from the knowledge of the reference flow, more specifically with the help of its velocity-gradient tensor and the rotation rate of the principal axes of its strain-rate tensor. The analytical diagnostics give the average barotropic conversion rate of kinetic energy from the basic flow to the perturbations in terms of alignment dynamics. We have shown that the alignment of the perturbation velocity vector can be expressed solely in terms of the properties of the basic flow. The paper was mainly motivated by the results of Mak and Cai (1989) concerning local barotropic instability. Cai and Mak (1990) then considered a case study where both barotropic and baroclinic processes govern the dynamics of the perturbations and analysed and explained the roles played by the different terms, especially the generation and redistribution terms involved in the local energy equations. In the same manner, the aim of the present paper is to generalize some results of RHK by analysing the relations between barotropic and baroclinic conversion terms. One of the main questions of the present paper is: can we analytically diagnose the most probable vertical structures and therefore the most probable baroclinic conversion rates with the help of the reference flow structure?

In RHK, the analogy with the dynamics of the horizontal tracer gradient growth has been fruitful because of the similarity between the linearized momentum equations for the perturbations in their Lagrangian form and the horizontal tracer gradient equations. Pursuing further the parallel between the tracer gradient growth and the velocity perturbation growth, we postulate that the relationship between the vertical and the horizontal structures of the perturbations is similar to that between the vertical and the horizontal distributions of the tracer gradient. The present paper is therefore motivated by the work of Haynes and Anglade (1997) who have shown that the vertical-scale cascade of the tracers occurs at the same rate as the horizontal-scale cascade. More specifically, they show that because of the interaction between the horizontal strain and the vertical shear, the vertical tracer gradients increase at the same exponential rate as the horizontal tracer gradients. In the same vein, Hua *et al.* (1998) show that the vertical distribution of the tracer gradients is completely constrained by the horizontal one. Exploiting the analogy with the three-dimensional (3D) aspect of the tracer gradient evolution, the issues addressed in the present paper concern the dependence of the vertical structure of the perturbations on their horizontal structure, on the basic-state horizontal deformation field and on the basic-state vertical shear. Such questions are related to the problem of the influence of the horizontal deformation field on the growth of baroclinic waves or frontal waves (Simmons and Hoskins 1980; James 1987; Bishop 1993; Bishop and Thorpe 1994; Snyder and Joly 1998, among others) which is complex when both horizontal straining and shearing terms act, and are not yet well understood.

In section 2, the evolution of the perturbation is expressed in terms of a unique equation describing the evolution of a 3D vector whose components are the spatial derivatives of the perturbation stream function. Analytical diagnostics of the preferred horizontal and vertical structures of the perturbations are inferred. Section 3 concerns numerical results about the most probable vertical structures of the perturbations,

the barotropic and baroclinic conversion terms, and the error fields. Section 4 provides a discussion of our results.

2. PERTURBATION EQUATIONS IN QG FLOWS

(a) Time evolution of the perturbation energy

The dynamics of perturbation growth are studied by writing the linearized momentum equations of a QG system. The chosen decomposition is the same as that adopted by Cai and Mak (1990) and Hua *et al.* (1998), in which the pressure field as well as the velocity field is decomposed into two parts, a geostrophic one and an ageostrophic one. The equations governing the perturbation (without the β-effect, whose influence is discussed later, and without viscous effects) are

$$\frac{\overline{D}\mathbf{u}'}{Dt} = -\nabla\overline{\mathbf{u}} \cdot \mathbf{u}' - \nabla p' - f_0\mathbf{k} \wedge \nabla\chi',$$ (1)

$$\frac{\partial w'}{\partial z} = -\triangle\chi',$$ (2)

$$\frac{\overline{D}}{Dt}(\partial_z\psi') = -(\mathbf{u}' \cdot \nabla)\partial_z\overline{\psi} - f_0 Sw',$$ (3)

where $\overline{D}/Dt = \partial/\partial t + (\overline{\mathbf{u}} \cdot \nabla)$ is the geostrophic total derivative, and $\mathbf{k}$ is the vertical unit vector. Overbars denote quantities associated with the reference flow, while primes denote perturbations. The geostrophic terms in these equations are the geostrophic velocity field, $\mathbf{u} = (u, v)$, the basic-state velocity-gradient tensor, $\nabla\overline{\mathbf{u}}$, and the geostrophic stream function, ψ. The ageostrophic terms included in (1), (2), (3), involve three terms: the field p' is the sum of the perturbation ageostrophic pressure field and a scalar function derived from the rotational part of the perturbation ageostrophic horizontal velocity, χ' is the gradient part of the perturbation ageostrophic horizontal velocity, and w' is the perturbation ageostrophic vertical velocity. Lastly, S is the mean stratification parameter. Both barotropic and baroclinic conversion terms will be analysed in terms of the alignment of a unique 3D vector, denoted $\mathbf{u}_3'$, whose components are those involved in the total perturbation energy, i.e. u', v' (related to the kinetic energy) and $(\partial_z\psi')/\sqrt{S}$ (related to the potential energy). Equations (1) and (3) may be rewritten as a 3D vector equation for $\mathbf{u}_3'$:

$$\frac{\overline{D}\mathbf{u}_3'}{Dt} = -\overline{\mathbf{A}} \cdot \mathbf{u}_3' - \nabla p' - f_0\mathbf{k} \wedge \nabla\chi' - f_0\sqrt{S}w'\mathbf{k},$$ (4)

where

$$\overline{\mathbf{A}} \equiv \begin{bmatrix} \partial_x\overline{u} & \partial_y\overline{u} & 0 \\ \partial_x\overline{v} & \partial_y\overline{v} & 0 \\ \frac{1}{\sqrt{S}}\partial_z\overline{v} & -\frac{1}{\sqrt{S}}\partial_z\overline{u} & 0 \end{bmatrix}, \quad \mathbf{u}_3' \equiv \begin{pmatrix} -\partial_y\psi' \\ \partial_x\psi' \\ \frac{1}{\sqrt{S}}\partial_z\psi' \end{pmatrix}.$$ (5)

The advantage of (4) is that the 3D perturbation properties can be studied by analysing the preferential alignments of the vector $\mathbf{u}_3'$, as was done for $\mathbf{u}'$ in RHK in a barotropic context. The normalization of the vertical coordinate, z, of $\mathbf{u}_3'$ by $\sqrt{S}$ relates its modulus to the perturbation total energy

$$\frac{|\mathbf{u}_3'|^2}{2} = \frac{1}{2}\left\{(\partial_x\psi')^2 + (\partial_y\psi')^2 + \left(\frac{1}{\sqrt{S}}\partial_z\psi'\right)^2\right\}.$$ (6)

By applying the operator $(-\partial_y., \partial_x., \partial_z(./\sqrt{S}))$ to Eq. (4), we obtain the linearized perturbation potential vorticity (PV) equation without the β-term

$$\frac{\overline{D}q'}{Dt} = -\mathbf{u}' \cdot \nabla \overline{q}, \tag{7}$$

where

$$q = \nabla^2 \psi + \partial_z \frac{1}{S} \partial_z \psi. \tag{8}$$

Let us now focus on the total energy equation deduced from Eq. (4) by taking its scalar product with $\mathbf{u}'_3$,

$$\frac{\partial}{\partial t} \frac{|\mathbf{u}'_3|^2}{2} = -\overline{\mathbf{u}} \cdot \nabla \frac{|\mathbf{u}'_3|^2}{2} - \nabla \cdot (p'\mathbf{u}') - \nabla \cdot (\psi' f_0 \nabla \chi') - \frac{\partial}{\partial z}(f_0 \psi' w')$$
$$+ \mathbf{E} \cdot \mathbf{D} + \mathbf{F}_h \cdot \mathbf{T}_h, \tag{9}$$

where

$$\mathbf{E} \equiv \{\tfrac{1}{2}(v'^2 - u'^2), -u'v'\},$$
$$\mathbf{D} \equiv (\partial_x \overline{u} - \partial_y \overline{v}, \partial_x \overline{v} + \partial_y \overline{u}), \tag{10}$$

and

$$\mathbf{F} \equiv (u', v', -w')\frac{1}{\sqrt{S}}\partial_z \psi',$$
$$\mathbf{T} \equiv \left(-\frac{1}{\sqrt{S}}\partial_z \overline{v}, \frac{1}{\sqrt{S}}\partial_z \overline{u}, f_0\sqrt{S}\right). \tag{11}$$

The definitions of the vectors $\mathbf{E}$, $\mathbf{D}$, $\mathbf{F}$ and $\mathbf{T}$ are introduced in Cai and Mak (1990). The two quantities $\mathbf{E} \cdot \mathbf{D}$ and $\mathbf{F}_h \cdot \mathbf{T}_h$ (where subscript h refers to the horizontal component of the vector), are respectively the barotropic and baroclinic conversion terms. The above paper details the equations for the kinetic energy and the potential energy and they are not recalled here. Let us just recall the physical interpretation of the terms that intervene in the total energy equation (9). The term $\mathbf{E} \cdot \mathbf{D}$ is called by Cai and Mak the barotropic energy generation rate because it enables the perturbation energy to grow globally by barotropic extraction, while the term $\mathbf{F}_h \cdot \mathbf{T}_h$ is the baroclinic energy generation rate that allows the perturbation to grow baroclinically. The vertical contribution term $-\mathbf{F}_3 \cdot \mathbf{T}_3$ represents the conversion rate from potential to kinetic energy and is thus not included in Eq. (9). The other terms $-\overline{\mathbf{u}} \cdot \nabla(|\mathbf{u}'_3|^2/2)$, $-\nabla \cdot (p'\mathbf{u}')$, $-\nabla \cdot (\psi' f_0 \nabla \chi')$ and $-\partial(f_0\psi'w')/\partial z$ are energy redistribution terms in horizontal space and a more detailed interpretation of each term can be found in Cai and Mak (1990).

(b)   *Barotropic and baroclinic conversion rates in terms of angles*

The aim of the present paper is not to analyse the different terms of the total energy equation, because it has already been done by Cai and Mak (1990), but to study the two orientation equations that follow from Eq. (4). The 3D vector $\mathbf{u}'_3$ is thus decomposed in spherical coordinates, θ', φ', as shown in Fig. 1. In these coordinates, the vector $\mathbf{u}'_3$ can be written as

$$\mathbf{u}'_3 = |\mathbf{u}'_3|(\cos\theta' \sin\varphi', \sin\theta' \sin\varphi', \cos\varphi') = |\mathbf{u}'_3|(\sin\varphi'\mathbf{e}' + \cos\varphi'\mathbf{k}) = |\mathbf{u}'_3|\mathbf{e}'_3, \tag{12}$$

with $\mathbf{e}'_3$ ($\mathbf{e}'$) denoting the unit vector pointing in the same direction as $\mathbf{u}'_3$ ($\mathbf{u}'$).
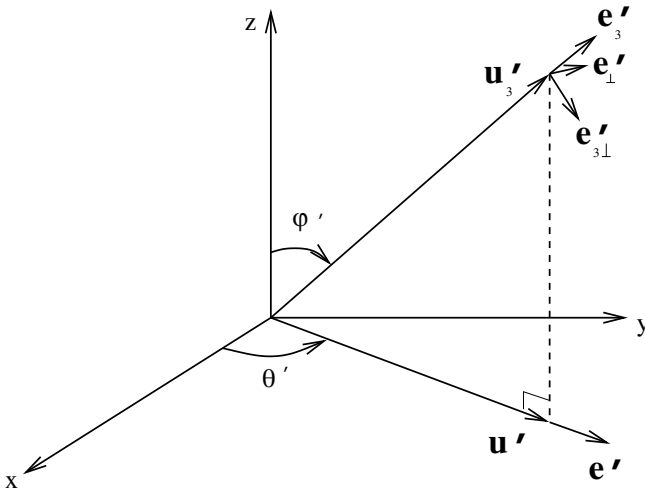
Figure 1. Angles defining the direction of the vector $\mathbf{u}_3'$.

Figure 1 summarizes the different definitions. The angle φ' is related to the ratio between the kinetic energy and potential energy of the perturbation

$$|\tan \varphi'| = \frac{|\mathbf{u}'|}{\left|\frac{1}{\sqrt{S}} \partial_z \psi'\right|}. \tag{13}$$

Furthermore, we use the notation introduced in RHK: the relative vorticity, normal and shear strain rates are respectively denoted $\overline{\omega} \equiv \partial_x \overline{v} - \partial_y \overline{u}$, $\overline{\sigma}_n \equiv \partial_x \overline{u} - \partial_y \overline{v}$ and $\overline{\sigma}_s \equiv \partial_x \overline{v} + \partial_y \overline{u}$. The angle $\overline{\phi}$ defined by $(\overline{\sigma}_s, \overline{\sigma}_n) = \overline{\sigma}(\cos 2\overline{\phi}, \sin 2\overline{\phi})$, determines the direction of the principal axes of the basic-state strain-rate tensor. Lastly, the angle $\zeta' \equiv 2(\theta' + \overline{\phi})$, related to the angle between the velocity perturbation and the compressional axis of strain, will also be used as it is crucial to determine the sign of the barotropic generation rate (see RHK). Other notation is needed to analyse the baroclinic generation rate, and so we define the vertical-shear strain rate, $\overline{\sigma}_z$, and the angle $\overline{\alpha}_z$ as

$$\left(\frac{1}{\sqrt{S}} \partial_z \overline{u}, \frac{1}{\sqrt{S}} \partial_z \overline{v}\right) = \overline{\sigma}_z(\cos \overline{\alpha}_z, \sin \overline{\alpha}_z), \tag{14}$$

with $\overline{\sigma}_z \geq 0$. The generation terms $\mathbf{E} \cdot \mathbf{D}$ and $\mathbf{F}_h \cdot \mathbf{T}_h$ can be written with our notation as

$$\mathbf{E} \cdot \mathbf{D} = -\frac{|\mathbf{u}_3'|^2}{2} \overline{\sigma} \sin^2 \varphi' \sin \zeta'$$

and

$$\mathbf{F}_h \cdot \mathbf{T}_h = \frac{|\mathbf{u}_3'|^2}{2} \overline{\sigma}_z \sin 2\varphi' \sin(\theta' - \overline{\alpha}_z).$$

These relations enable us to define the following exponential generation rates for the total energy of the perturbations

$$\delta^{\mathrm{b}} \equiv \frac{\mathbf{E} \cdot \mathbf{D}}{0.5|\mathbf{u}_3'|^2} = -\overline{\sigma} \sin^2 \varphi' \sin \zeta', \tag{15}$$

$$\delta^{\mathrm{c}} \equiv \frac{\mathbf{F}_{\mathrm{h}} \cdot \mathbf{T}_{\mathrm{h}}}{0.5|\mathbf{u}_3'|^2} = \overline{\sigma}_z \sin 2\varphi' \sin(\theta' - \overline{\alpha}_z), \tag{16}$$

$$\delta^{\mathrm{t}} \equiv \delta^{\mathrm{b}} + \delta^{\mathrm{c}}. \tag{17}$$

δ^{b} is the barotropic exponential generation rate of energy, δ^{c} the baroclinic exponential generation rate of energy and δ^{t} the total exponential generation rate of energy. The term exponential is used in these definitions because δ^{b} and δ^{c} appear when we divide Eq. (9) by $0.5|\mathbf{u}_3'|^2$ to obtain the exponential energy growth rate. Let us analyse δ^{c}. In the simple baroclinic situation of a zonal jet with a positive vertical shear, we have $\partial_z \overline{v} = 0$ and $\partial_z \overline{u} > 0$, which lead to $\overline{\alpha}_z = 0$. In order to obtain a positive baroclinic growth rate, $\delta^{\mathrm{c}} > 0$, the condition $\sin \theta' \sin 2\varphi' > 0$ is required (see Eq. (16)) which leads to $\partial_x \psi' \partial_z \psi' > 0$. We recover the usual condition for perturbation growth—the structure of the perturbation must lean against the shear. The physical interpretation of the exponential barotropic generation rate of total energy has already been analysed in RHK since δ^{b} is directly related to $\delta \equiv -\overline{\sigma} \sin \zeta'$, the exponential generation rate of kinetic energy ($\delta^{\mathrm{b}} = \delta \sin^2 \varphi'$). In order to assess the relative importance of baroclinic processes with respect to barotropic ones, we introduce the ratio of the barotropic generation rate over the baroclinic one

$$R^{\mathrm{bc}} \equiv \frac{\mathbf{E} \cdot \mathbf{D}}{\mathbf{F}_{\mathrm{h}} \cdot \mathbf{T}_{\mathrm{h}}} = \frac{\delta^{\mathrm{b}}}{\delta^{\mathrm{c}}}. \tag{18}$$

The barotropic and baroclinic conversion rates of basic-state energy into perturbation energy (Eqs. (15) and (16)) require the explicit orientation (θ' and φ') of the perturbation in terms of properties of the reference flow. This is the focus of the next section.

(c) *Approximation of the orientation equations*

The 3D vector equation (4) can be decomposed into three scalar equations. One equation describes the evolution of the modulus of $\mathbf{u}_3'$ (i.e the total energy equation (9)) and is obtained by projection on the unit vector $\mathbf{e}_3'$. The other two equations, which result from a projection on unit vectors $\mathbf{e}_{3\perp}' \equiv \cos \varphi' \mathbf{e}' - \sin \varphi' \mathbf{k}$ and $\mathbf{e}_\perp' \equiv (-\sin \theta', \cos \theta')$, determine the time evolution of the orientation of $\mathbf{u}_3'$. The projection of the first term on the right-hand side of Eq. (4) on $\mathbf{e}_{3\perp}'$ and $\mathbf{e}_\perp'$ can be easily obtained but, as in RHK, the problem concerns the projection of the ageostrophic terms on the two unit vectors. Hereafter, we will call $-\nabla p'$ the barotropic ageostrophic vector, denoted as $\mathbf{v}_p$. The vector $-f_0 \mathbf{k} \wedge \nabla \chi' - f_0 \sqrt{S} w' \mathbf{k}$ will be called the baroclinic ageostrophic vector, denoted as $\mathbf{v}_{\chi,w}$. The purpose of the following paragraph is to obtain simple analytical expressions for the projections of $\mathbf{v}_p$ and $\mathbf{v}_{\chi,w}$ onto $\mathbf{e}_{3\perp}'$ and $\mathbf{e}_\perp'$.

By manipulating Eqs. (2) and (4), it is straightforward to obtain the linearized ageostrophic terms p', χ', w',

$$\triangle p' = 2\{J_{xy}(\overline{u}, v') + J_{xy}(u', \overline{v})\}, \tag{19a}$$

$$\left(\triangle + \partial_z \frac{1}{S} \partial_z\right) \triangle f_0 \chi' = -2\partial_z \frac{1}{S} \nabla \cdot \mathbf{Q}', \tag{19b}$$

$$\left(\triangle + \frac{1}{S}\partial_z^2 \right) w' = \frac{2}{f_0 S}\nabla \cdot \mathbf{Q}', \tag{19c}$$

where

$$\mathbf{Q}' \equiv (J_{zx}, J_{zy})(\overline{u}, v') + (J_{zx}, J_{zy})(u', \overline{v}) \tag{20}$$

is the linearized version of the vector $\mathbf{Q} \equiv -J_{xy}(\nabla\psi, \partial_z\psi)$ introduced by Hoskins, Draghici and Davies (1978) and where $J_{ij}(a, b) \equiv \partial_i a \partial_j b - \partial_j a \partial_i b$ is the Jacobian operator. Some insight into the local dynamical influence of the ageostrophic terms may be obtained by using Eq. (19) for the simple case of a monochromatic perturbation

$$\psi'(x, y, z) = \text{Re}[A \exp\{i(kx + ly + mZ)\}], \tag{21}$$

where the Z-coordinate is related to the vertical coordinate, z, by $\partial Z/\partial z = 1/\sqrt{S}$, and k, l, m are wave numbers. We will consider the coefficients of the matrix $\overline{\mathbf{A}}$ as slowly varying and S to be a constant. The relation obtained in RHK for the perturbation ageostrophic pressure gradient still holds (see section 2(c) of RHK); the pressure gradient only projects on $\mathbf{e}'_\perp$ and thus modifies the orientation equation for θ'

$$\frac{\mathbf{v}_p \cdot \mathbf{e}'_\perp}{|\mathbf{u}'|} = \overline{\sigma}(\cos \zeta' + r_{\text{ow}}), \tag{22}$$

where

$$r_{\text{ow}} \equiv \frac{\overline{\omega}}{\overline{\sigma}}. \tag{23}$$

The subscript 'ow' follows the same terminology as RHK and refers to the Okubo–Weiss criterion. The steps leading to the expression of the baroclinic ageostrophic vector are not developed here since they are analogous to those described in section 2(c) of RHK. The baroclinic ageostrophic vector has no projection on either $\mathbf{e}'_3$ or $\mathbf{e}'_\perp$, but has a non-trivial projection on $\mathbf{e}'_{3\perp}$:

$$\frac{\mathbf{v}_{\chi,w} \cdot \mathbf{e}'_{3\perp}}{|\mathbf{u}'_3|} = 2\sin\varphi' \left\{ \frac{\overline{\sigma}}{2}\sin\zeta'\cos\varphi' + \overline{\sigma}_z \sin(\theta' - \overline{\alpha}_z)\sin\varphi' \right\}. \tag{24}$$

The main result of our analytical approach, based on a monochromatic perturbation and a WKB assumption, is that the two ageostrophic vectors, $\mathbf{v}_p$ and $\mathbf{v}_{\chi,w}$, locally influence the orientation of the vector $\mathbf{u}'_3$ but do not modify its norm. The barotropic ageostrophic vector, $\mathbf{v}_p$, modifies the horizontal orientation of $\mathbf{u}'_3$, while the baroclinic ageostrophic vector, $\mathbf{v}_{\chi,w}$, modifies its vertical orientation. With the above assumptions, the ageostrophic redistribution terms in the total energy equation are trivial and equal to zero. This is not the case generally (see Cai and Mak 1990). A weakness of our present approach is the absence of diagnostics of the ageostrophic horizontal redistribution terms, yet it provides an analytical approximation of the ageostrophic terms that intervene in the orientation equations of the vector $\mathbf{u}'_3$. In section 3(a)(v), the consistency of our approach is checked numerically.

The equation for the perturbation norm and the two orientation equations have thus the following form:

$$\frac{1}{|\mathbf{u}'_3|^2}\frac{\overline{D}|\mathbf{u}'_3|^2}{Dt} = -\overline{\sigma}\sin\zeta'\sin^2\varphi' + \overline{\sigma}_z \sin(\theta' - \overline{\alpha}_z)\sin 2\varphi', \tag{25a}$$

$$\frac{\overline{D}\theta'}{Dt} = -\frac{\overline{\sigma}}{2}(r_{\text{ow}} + \cos\zeta') + \frac{\mathbf{v}_p \cdot \mathbf{e}'_\perp}{|\mathbf{u}'|} = \frac{\overline{\sigma}}{2}(r_{\text{ow}} + \cos\zeta'), \tag{25b}$$

$$\frac{\overline{D}\varphi'}{Dt} = -\sin\varphi' \left\{ \frac{\overline{\sigma}}{2} \sin\zeta' \cos\varphi' + \overline{\sigma}_z \sin(\theta' - \overline{\alpha}_z) \sin\varphi' \right\} + \frac{\mathbf{v}_{\chi,w} \cdot \mathbf{e}'_{3\perp}}{|\mathbf{u}'_3|}$$

$$= \sin\varphi' \left\{ \frac{\overline{\sigma}}{2} \sin\zeta' \cos\varphi' + \overline{\sigma}_z \sin(\theta' - \overline{\alpha}_z) \sin\varphi' \right\}. \tag{25c}$$

We find that the time evolution for the angles θ' and φ' does not depend on the strength of the perturbation $|\mathbf{u}'_3|^2$. Moreover, in a monochromatic context, by assuming that the coefficients of the matrix $\overline{\mathbf{A}}$ are slowly varying, we remark that the projection of the ageostrophic terms on the two orientation equations for θ' and φ' is twice the opposite value of the projection of $-\overline{\mathbf{A}} \cdot \mathbf{u}'_3$. Let us note a property that comes from the degenerate form of the matrix $\overline{\mathbf{A}}$: from Eqs. (25b) and (25c), we deduce that the time evolution of the horizontal structure, i.e. $\overline{D}\theta'/Dt$, depends only on the horizontal structure itself (θ') whereas the evolution of the vertical structure, i.e. $\overline{D}\varphi'/Dt$, is dependent on both the horizontal structure θ' and the vertical structure φ'. The same properties have been shown by Hua *et al.* (1998) for the 3D tracer gradient, whose evolution depends on a degenerate matrix very similar to $\overline{\mathbf{A}}$ and whose vertical distribution is completely constrained by the horizontal one, while the reverse is not true.

The 2D case studied in RHK can be recovered from Eqs. (25a) and (25b); if the vertical derivatives are assumed to be zero, $|\mathbf{u}'_3|^2/2 = |\mathbf{u}'|^2/2$ is just the perturbation kinetic energy and the vertical angle φ' is trivially equal to $\pi/2$. Under these assumptions, Eqs. (25a) and (25b) are respectively identical to Eqs. (15a) and (26) of RHK.

(d) *Preferred orientations for the 3D perturbation stream-function gradient*

In RHK, preferred orientations for the perturbation velocity vector have been found by studying Lagrangian equilibria of the perturbation velocity vector orientation in two different reference frames, the laboratory frame and the basic-flow strain coordinates frame. These preferred orientations for $\mathbf{u}'$ are still valid as Eq. (26) of RHK and the general 3D case Eq. (25b) for θ' are strictly identical.

The Lagrangian equilibrium in strain coordinates satisfies $\overline{D}\zeta'/Dt = 0$ and the associated preferred values for θ' is given by

$$\theta' = \theta^r_\pm \equiv \tfrac{1}{2}(\zeta^r_\pm - 2\overline{\phi}) \equiv \tfrac{1}{2}\{\pm\arccos(-r) - 2\overline{\phi}\}, \tag{26}$$

where $r \equiv (\overline{\omega} + 2\overline{D}\overline{\phi}/Dt)/\overline{\sigma}$ (see RHK for further details). This solution would be analytically exact if r was a constant along a Lagrangian path. For the flow considered in RHK and in section 3 of the present paper, the parameter r is actually slowly varying along the strong energetic jet and around the few large isolated vortices which are the two most energetic structures of the flow. The definition of r involves the basic-state relative vorticity, the basic-state strain rate and the rotation rate of the strain axes, $2\overline{D}\overline{\phi}/Dt$, which is added to the effect of relative vorticity. The $2\overline{D}\overline{\phi}/Dt$ term is obtained from a diagnostic equation in which the basic-state ageostrophic pressure intervenes (see Eqs. (7a) and (7b) of Lapeyre *et al.* 1999). The quantitative importance of $2\overline{D}\overline{\phi}/Dt$ depends on the nature of the flow (e.g. the existence of coherent curved structures (Lapeyre *et al.* 1999)) and may become smaller in more rectilinear jet-like flows such as the one considered in RHK.

The Lagrangian equilibrium in the laboratory reference frame corresponds to the solutions of the equation $\overline{D}\theta'/Dt = 0$ and is determined by the angle of $\mathbf{u}'$ with respect to the x-axis:

$$\theta' = \theta^{row}_\pm \equiv \tfrac{1}{2}(\zeta^{row}_\pm - 2\overline{\phi}) \equiv \tfrac{1}{2}\{\pm\arccos(-r_{ow}) - 2\overline{\phi}\}. \tag{27}$$

This equation can be deduced from (26) whenever $2\overline{D}\,\overline{\phi}/Dt$ is negligible. RHK found that r is relevant in regions of large $\mathbf{E} \cdot \mathbf{D}$, while r_{ow} prevails for large exponential growth rate, δ^b.

The main purpose of the present paper is to determine the preferred values for the vertical angle φ'. Two types of preferred values can be found according to the chosen reference frame. For simplicity, we have opted for the laboratory reference frame, i.e. $\overline{D}\theta'/Dt = 0$ and $\overline{D}\varphi'/Dt = 0$. The orientations satisfying these two equations correspond to those of the eigenvectors of the matrix $\overline{\mathbf{A}}$ whose eigenvalues are real if $|r_{ow}| < 1$. The angle θ' is given by the values $\theta_{\pm}^{row}$ (see Eq. (27)) and the angle φ' is given by

$$\varphi_{\pm}^{row} = \arctan\left[\mp \frac{\frac{1}{2}\sqrt{\overline{\sigma}^2 - \overline{\omega}^2}}{\overline{\sigma}_z \sin\left\{\pm\frac{1}{2}\arccos(-\overline{\omega}/\overline{\sigma}) - \overline{\phi} - \overline{\alpha}_z\right\}}\right]. \tag{28}$$

The angle θ_-^{row} induces barotropic growth and θ_+^{row} barotropic decay. In the following, we will refer to directions of the velocity perturbation that lead to growth (decay) as productive (destructive). The additional information given by the eigenvectors of $\overline{\mathbf{A}}$ concerns the vertical structure and the associated baroclinic processes. For $|r_{ow}| < 1$, there exist two preferential vertical directions, $\varphi' = \varphi_{\pm}^{row}$, corresponding to the two eigenvectors with non-zero eigenvalues: φ_-^{row} implies baroclinic growth and φ_+^{row} baroclinic decay. The eigenvector direction determined by the couple $(\theta_-^{row}, \varphi_-^{row})^*$ corresponds to perturbation growth due to both barotropic and baroclinic growth. The corresponding exponential generation rates are

$$\delta_{ow}^b \equiv -\overline{\sigma}\sin\zeta_-^{row}\sin^2\varphi_-^{row} > 0, \tag{29a}$$

$$\delta_{ow}^c \equiv \overline{\sigma}_z \sin 2\varphi_-^{row}\sin(\theta_-^{row} - \overline{\alpha}_z) = -\overline{\sigma}\sin\zeta_-^{row}\cos^2\varphi_-^{row} > 0, \tag{29b}$$

$$\delta_{ow}^t \equiv -\overline{\sigma}\sin\zeta_-^{row} = \sqrt{\overline{\sigma}^2 - \overline{\omega}^2} > 0, \tag{29c}$$

while the eigenvector direction determined by the couple $(\theta_+^{row}, \varphi_+^{row})$ leads to perturbation decay. We remark that the total exponential generation rate of the eigenvectors δ_{ow}^t depends only on the horizontal components of the basic-state tensor $\overline{\mathbf{A}}$ because of its degenerate form. However this does not mean that baroclinic processes are less effective than barotropic ones; for example, if $0 < \varphi_-^{row} < \pi/4$, we have $\delta_{ow}^c > \delta_{ow}^b$ and the baroclinic conversion rate is larger than the barotropic one.

An analytical estimate of the ratio between barotropic and baroclinic generation rates R^{bc} is given by the productive eigenvector structure of $\overline{\mathbf{A}}$

$$R_{ow}^{bc} \equiv \frac{\delta_{ow}^b}{\delta_{ow}^c} = \tan^2\varphi_-^{row} = \frac{\frac{1}{4}(\overline{\sigma}^2 - \overline{\omega}^2)\left\{(\overline{\sigma}_s - \overline{\omega})^2 + \left(\overline{\sigma}_n + \sqrt{\overline{\sigma}^2 - \overline{\omega}^2}\right)^2\right\}}{\left\{\frac{1}{\sqrt{S}}\partial_z\overline{u}\left(\overline{\sigma}_n + \sqrt{\overline{\sigma}^2 - \overline{\omega}^2}\right) + \frac{1}{\sqrt{S}}\partial_z\overline{v}(\overline{\sigma}_s - \overline{\omega})\right\}^2}, \tag{30}$$

which also corresponds exactly to the ratio of the kinetic energy to the potential energy of the perturbation for the same structure (see Eq. (13)). Indeed, if $\varphi' \simeq \varphi_-^{row}$, we have both $|\mathbf{u}'|^2/(1/S|\partial_z\psi'|^2) = \tan^2\varphi' \simeq \tan^2\varphi_-^{row}$ and $R^{bc} \simeq R_{ow}^{bc} = \tan^2\varphi_-^{row}$, i.e. for the productive eigenvector structure, the ratio of the kinetic energy to the potential energy

---

* Each couple $(\theta_-^{row}, \varphi_-^{row})$ and $(\theta_+^{row}, \varphi_+^{row})$ defines only one possible orientation of the direction of each eigenvector; the other orientation is given by $(\theta_-^{row} + \pi, \pi - \varphi_-^{row})$ and $(\theta_+^{row} + \pi, \pi - \varphi_+^{row})$.

of the perturbation is equal to the ratio of the barotropic conversion term to the baroclinic one.

The ageostrophic terms' contributions in the orientation equations are zero for the eigenvectors' directions; with or without these terms the preferred orientations determined by $\overline{D}\theta'/Dt = 0$ and $\overline{D}\varphi'/Dt = 0$ remain unchanged. However, taking into account the ageostrophic terms modifies the stability of the solutions; the direction corresponding to the eigenvector direction $(\theta_-^{row}, \varphi_-^{row})$ $((\theta_+^{row}, \varphi_+^{row}))$, which is stable (unstable) without the ageostrophic terms, becomes unstable (stable) in their presence. (See appendix A of RHK for the stability analysis.) Furthermore, this stability property will be emphasized in the simple analytical cases of the next section.

By taking into account the β-effect, analytical calculations similar to those of appendix B of RHK show that, for a monochromatic perturbation, the orientation equations are not modified (only the equation of $|\mathbf{u}_3'|$ is changed), and the eigenvectors' directions $(\theta_-^{row}, \varphi_-^{row})$ and $(\theta_+^{row}, \varphi_+^{row})$ are thus still preferred directions for any QG flows on a β-plane.

(e)   Discussion

A class of analytical solutions exactly verifies the approximations made in section 2(c) and therefore satisfies Eqs. (25a–c); they are composed of monochromatic disturbances with time-dependent wave numbers superimposed on a basic flow whose velocity components are linearly dependent on spatial coordinates. Furthermore, Craik and Criminale (1986) have shown that such solutions satisfy the incompressible Navier–Stokes equations. In atmospheric sciences, two well-known limiting cases, the Orr (1907) mechanism and the pure strain case studied by Farrell (1989), correspond to particular examples of these analytical solutions. In this section, we revisit these two cases to identify the preferred orientations of the perturbations defined in section 2(d) and to compare them with the classical optimal orientations of the singular vectors (Farrell and Ioannou 1996). The end of the section is devoted to the relationship between the horizontal and vertical structures.

(i)   *The Orr case.*   The Orr (1907) mechanism is a well-known case of non-modal transient growth where perturbations grow temporarily as long as their spatial structures tilt against the shear. In this case, the flow is zonal and meridionally sheared, $\overline{\mathbf{u}} = Sy\,\mathbf{e}_x$, with $S > 0$ and the different quantities defined in section 2(c) are $\overline{\omega} = -S$, $\overline{\sigma}_s = S$, $\overline{\sigma}_n = 0$, $\overline{\sigma} = S$, $2\overline{\phi} = 0$ and $r = r_{ow} = -1$. Equations (25a) and (25b) can be completely solved by integration along a Lagrangian path and lead to

$$\zeta' = \pi + 2\arctan(A_0 - \overline{\sigma}t), \tag{31a}$$

$$|\mathbf{u}'|^2 = |\mathbf{u}'|_0^2 \frac{1 + A_0^2}{1 + (A_0 - St)^2}, \tag{31b}$$

where the subscript 0 denotes values at initial time and $A_0 = \tan(\theta_0' + \pi/2) = l_0/k_0$ for a monochromatic perturbation with initial wavenumber (k_0, l_0). Equation (31b) illustrates the classical algebraic amplification of the perturbation kinetic energy in the Orr case which has been recovered for our approach. The fixed points of the orientation equation (27) (or equivalently (26)) in the Orr case are determined by $\theta_\pm^r = \theta_\pm^{row} = 0$, i.e. the two fixed points coincide with the x-axis orientation. The strain dilatation (contraction) axis is defined by $\theta' = \pi/4$ ($\theta' = -\pi/4$), i.e. it corresponds to the first (second) bisecting line of the x, y coordinates. The fixed points of the orientation equation thus differ from the strain dilatation and contraction axes. If the perturbation

isolines have a slightly negative slope, perturbations will extract energy from the basic flow but will move away from the x-axis, i.e. from the productive fixed point $\theta^r_- = \theta^{row}_-$. In the same manner, if the perturbation isolines have a slightly positive slope, their kinetic energy is destroyed and their orientation will evolve toward the x-axis, i.e. the destructive fixed point in this case. We have thus recovered in the Orr case the general fact that the productive fixed point is unstable and the destructive one stable.

(ii) *The pure strain case.* Farrell (1989) has shown that a specific configuration of the perturbations in a pure strain can yield an exponential transient growth. The basic-flow stream function determined by $\overline{\psi} = S(x^2 - y^2)/4$ represents a pure horizontal strain and leads to $\overline{\omega} = 0, \overline{\sigma}_s = S, \overline{\sigma}_n = 0, \overline{\sigma} = S$ and $2\overline{\phi} = 0$. Since the relative vorticity and $2\overline{\phi}$ are zero, $r = r_{ow} = 0$. By integrating Eqs. (25a) and (25b), this leads to

$$\zeta' = -\pi/2 + 2\arctan(e^{A_0 + \overline{\sigma}t}), \tag{32a}$$

$$|\mathbf{u}'|^2 = |\mathbf{u}'|^2_0 \frac{\cosh(A_0)}{\cosh(A_0 + \overline{\sigma}t)}, \tag{32b}$$

with $A_0 = \tan(\theta'_0 + \pi/2) = l_0/k_0$ for a monochromatic perturbation with initial wavenumber (k_0, l_0). Perturbation transient growth occurs if k_0 and l_0 have the same sign, as in the Orr case, but the difference is that, in the pure strain case, the growth is exponential. The exponential dependence on time in Eq. (32b) corresponds to the expression found by Farrell (1989). Recently, Iacono (2002) generalized this result by showing that, for any perturbation, its initial energy growth rate only depends on the global shape of the perturbation and the basic-flow strain rate. By contrast with the Orr case, the productive and destructive fixed points, $\theta^r_- = \theta^{row}_- = -\pi/4$ and $\theta^r_+ = \theta^{row}_+ = \pi/4$ respectively coincide with the contraction and dilatation axes. We find again in this limiting case that the destructive fixed point is a stable orientation and the productive fixed point an unstable one.

From the two simple cases described above, the importance of the parameter r (or equivalently r_{ow})* for characterizing perturbation growth is clearly shown; if $|r| = 1$, the transient growth is algebraic whereas if $|r| < 1$, it is exponential.

Furthermore, these two cases enable one to distinguish between preferential orientations defined by Lagrangian equilibria on the one hand and optimal orientations for perturbation growth predicted by singular vectors on the other. Indeed, the strain contraction axis is the orientation of the singular vector that optimizes at short times and is different from the preferred productive orientation θ^r_- in the general case where $r \neq 0$. It is only for the pure strain case, for which r is zero, that the two orientations are identical.

(iii) *Link between horizontal and vertical structures.* Let us revisit the 3D case studied by Haynes and Anglade (1997), hereafter HA97, in their section 2. Their case involves a vertical shear $\overline{\sigma}_z$ and a pure horizontal strain $\overline{\sigma}$, the velocity components are defined by $(u, v) = (\Gamma x, -\Gamma y + \Lambda z)$ and leads to $\overline{\omega} = 0, \overline{\sigma}_s = 0, \overline{\sigma}_n = 2\Gamma, \overline{\sigma} = 2\Gamma,$ $2\overline{\phi} = \pi/2, r = r_{ow} = 0, \overline{\sigma}_z = \Lambda$ and $\overline{\alpha}_z = \pi/2$. HA97 considered a monochromatic form for the PV field, and showed that the vertical and horizontal wave numbers m and $\sqrt{k^2 + l^2}$ increase exponentially for long times but the ratio of vertical to horizontal scales, $|m|/\sqrt{k^2 + l^2}$, tends toward the value $\Gamma/\Lambda = \overline{\sigma}/(2\overline{\sigma}_z)$, i.e. toward half the ratio of horizontal strain rate to vertical shear. This ratio can be recovered directly from

* Note that in both the Orr case and the pure strain case, the strain axes do not change and there is no difference between $\theta^r_\pm$ and $\theta^{row}_\pm$.

the preferential destructive orientation defined in Eq. (28), $\tan \varphi_+^{row} = m/\sqrt{k^2 + l^2} = \overline{\sigma}/(2\overline{\sigma_z})$, by setting $\overline{\omega} = 0$, $\overline{\phi} = \pi/4$ and $\overline{\alpha}_z = \pi/2$.

HA97 have generalized this result to more general flows in terms of typical horizontal strain rate and typical vertical shear. Consequently, their conclusion that the vertical structure is slaved to the horizontal ones through the ratio $\overline{\sigma}/(2\overline{\sigma_z})$ applies to our results as well. However, our Eq. (28) (or equivalently Eq. (30)) is more general and is an explicit function at each point of physical space of the 3D local structure of the basic flow that takes into account the relative vorticity, the horizontal normal and shear straining rates as well as the vertical zonal and meridional shear rates. The aim of the next section is especially to validate numerically the relevance of the analytical estimate (Eq. (30)).

3. NUMERICAL RESULTS IN A QG MODEL

As in RHK, results are given for the classical oceanic case of a wind-driven double gyre obtained with a 6-layer QG code in a rectangular basin. An illustration of the reference flow is shown in Fig. 1 of RHK and detailed information about the numerical code is given in their appendix C. The same ensemble of 200 random perturbations that have evolved for 20 days* is used here. Even if our analytical results are derived with linearized equations, we stress that the numerical results are performed with multiple runs of the fully nonlinear model, i.e. each perturbation at T = 20 days is defined as the difference between two runs of the nonlinear code—a perturbed run and the reference run. All numerical results are obtained for perturbations within the area A at the end part of the jet (see Fig. 1 of RHK).

(a) *Alignment dynamics in regions of large total-energy extraction*

(i) *Vertical slope of the perturbation isolines.* We first want to check numerically if the vertical structure defined by the eigenvector of $\overline{\mathbf{A}}$ corresponding to perturbation growth $(\theta_-^{row}, \varphi_-^{row})$ is the most probable vertical structure of the perturbations. As the eigenvector defines a direction property and not an orientation, we have to compare (θ', φ') with both $(\theta_-^{row}, \varphi_-^{row})$ and $(\theta_-^{row} + \pi, \pi - \varphi_-^{row})$. Probability density functions (PDFs) determining the most probable angle, ζ', are plotted in RHK and θ_-^{row} and $\theta_-^{row} + \pi$ are represented by the same angle $\zeta_-^{row} = 2(\theta_-^{row} + \overline{\phi}) = 2(\theta_-^{row} + \pi + \overline{\phi})$. In Fig. 2, PDFs of $\varphi' - \pi/2$ and $\varphi' - \varphi_-^{row}$ are shown, where the difference in angles has been taken modulo π because of the above remark on direction and orientation.

The PDF of $\varphi' - \pi/2$ in Fig. 2(a) shows that in the first layer, φ' is overall close to $\pi/2$, meaning that the perturbation is mostly horizontal and that the perturbation kinetic energy is stronger than the potential one. However the PDF of $\varphi' - \pi/2$ does not present a sharp peak while a non-trivial vertical structure exists which is clearly much better diagnosed by the orientation φ_-^{row} as shown by the PDF of $\varphi' - \varphi_-^{row}$ in Fig. 2(a). There is therefore a clear alignment of φ' with the direction defined by φ_-^{row} in the first layer. This result is comparable to the result of Fig. 3 in RHK, which shows that θ' aligns with θ_-^{row}. In the second layer (Fig. 2(b)), the alignment of φ' with φ_-^{row} is also present, but has a less strong peak than in the first layer. The PDF of $\varphi' - \pi/2$ in Fig. 2(b) shows that, by contrast with the first layer, the perturbation structure in the second layer departs from a horizontal structure and therefore has almost as much potential energy as kinetic energy.

---

* Results reported here concern baroclinic processes and correspond to longer finite time diagnostics than in RHK who used only 10-day integrations for diagnosing barotropic instability.
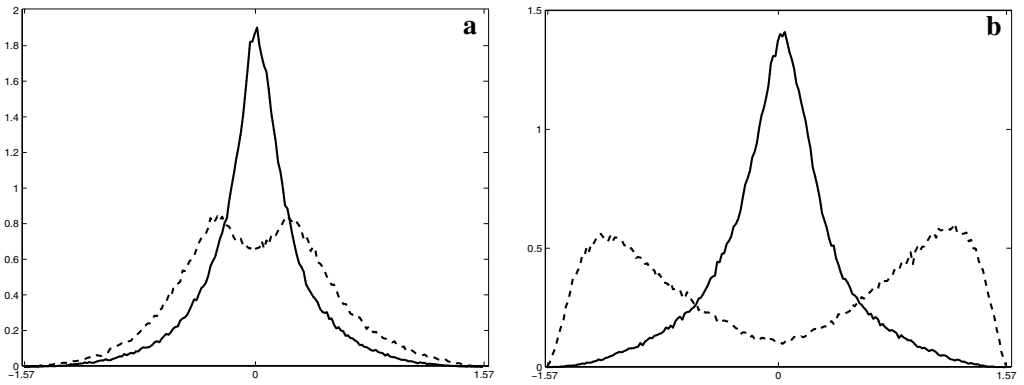
Figure 2. The probability density function at T = 20 days of $\varphi' - \pi/2$ (dashed line) and $\varphi' - \varphi_-^{r_{ow}}$ (solid line), conditioned by $|r_{ow}| < 1$ and $\mathbf{E} \cdot \mathbf{D} + \mathbf{F}_h \cdot \mathbf{T}_h > |\mathbf{E} \cdot \mathbf{D} + \mathbf{F}_h \cdot \mathbf{T}_h|_{max}/100$; in the (a) first layer and (b) second layer (see text for details). This statistic is obtained from an ensemble of 200 perturbations.
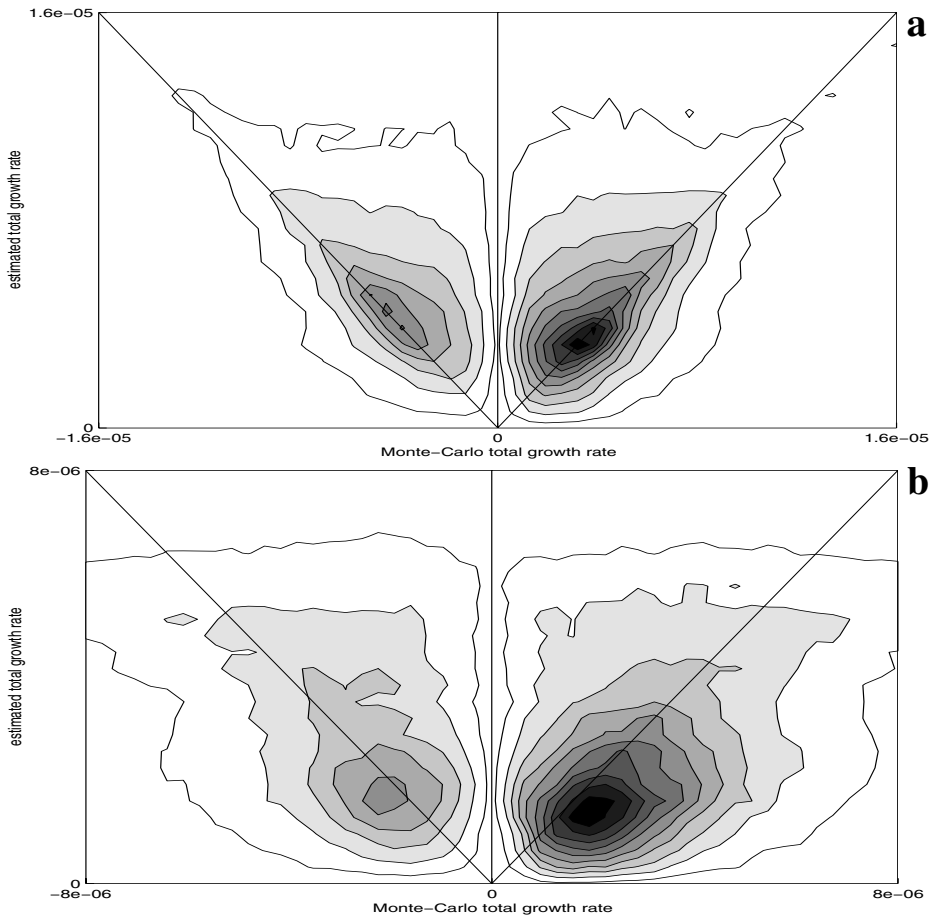

Figure 3. The joint probability density function at T = 20 days of the total-energy Monte-Carlo growth rate, δ^t, with the estimate δ^t_{ow}, conditioned by $|r_{ow}| < 1$ and $|\mathbf{E} \cdot \mathbf{D} + \mathbf{F}_h \cdot \mathbf{T}_h| > |\mathbf{E} \cdot \mathbf{D} + \mathbf{F}_h \cdot \mathbf{T}_h|_{max}/200$; in the (a) first layer and (b) second layer (see text for details).
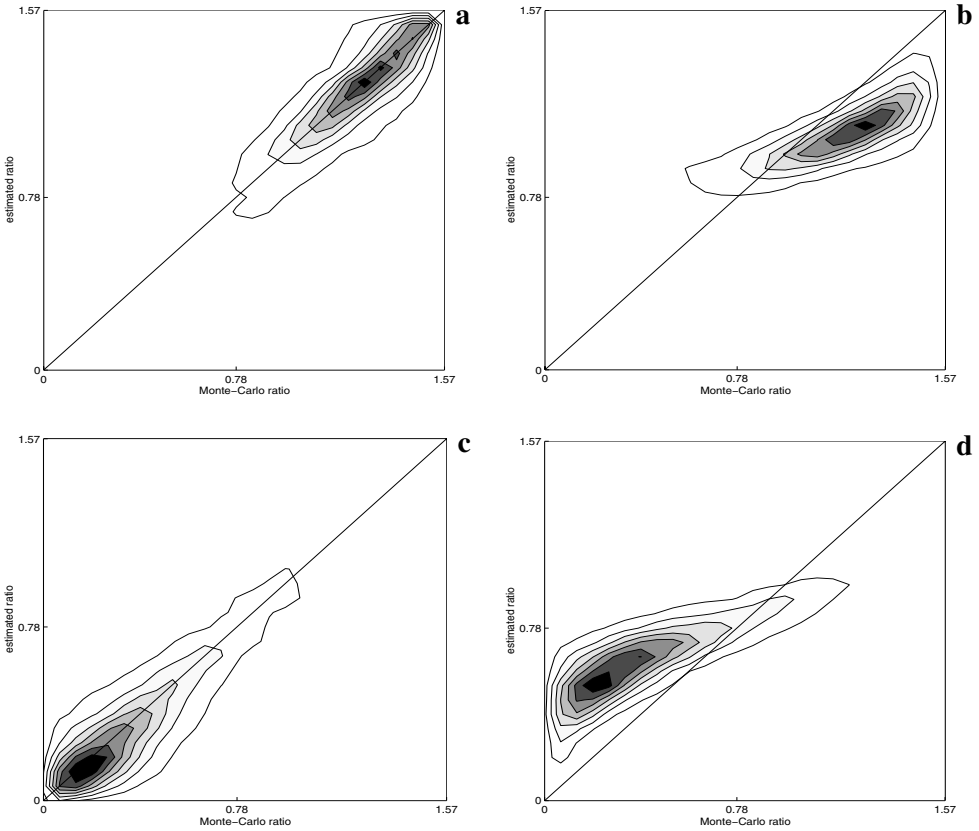
Figure 4. Joint probability density functions (PDFs) at $T = 20$ days of the Monte-Carlo ratio between the barotropic generation rate and the baroclinic generation rate, $\arctan(\sqrt{|R^{bc}|})$, with two analytical estimations: one with the estimate, $\arctan(\sqrt{R^{bc}_{ow}})$, diagnosed by our approach, in the (a) first layer and (c) second layer; the other with the simplified estimate, $\arctan(\sqrt{\overline{\sigma}/\sigma_z})$, in the (b) first layer and (d) second layer (see text for details). The joint PDFs are conditioned by $|r_{ow}| < 1$ and $\mathbf{E} \cdot \mathbf{D} + \mathbf{F}_h \cdot \mathbf{T}_h > |\mathbf{E} \cdot \mathbf{D} + \mathbf{F}_h \cdot \mathbf{T}_h|_{max}/100$.

(ii)   *Total exponential generation rate of energy.*   In section 2(d), we computed the total-energy exponential generation rate, δ^t_{ow}, for the eigenvector direction. A comparison with the actual Monte-Carlo generation rate, δ^t, for 200 perturbations is performed in Fig. 3. In the two layers, most points are clustered near the bisector of the right quadrant (productive direction); the correlation is better in the first layer than in the second one, a result already noted for the PDFs of Fig. 2. As in RHK for the kinetic-energy generation rate, there exists a less pronounced branch in the left quadrant. This second branch means that a non-negligible ratio of the couple points (θ', φ') is very close to the destructive structure determined by the couple $(\theta^{r_{ow}}_+, \varphi^{r_{ow}}_+)$. The relative importance of $(\theta^{r_{ow}}_+, \varphi^{r_{ow}}_+)$ and $(\theta^{r_{ow}}_-, \varphi^{r_{ow}}_-)$ has been found to be sensitive to the spatial scale of the random perturbations of the Monte-Carlo technique (not shown here).

(iii)   *Ratio between barotropic and baroclinic generation rates.*   We investigate now the ratio, R^{bc}, of the barotropic conversion term to the baroclinic one, defined in section 2(b). Figures 4(a) and (c) show the joint PDF of $\arctan(\sqrt{|R^{bc}|})$ with the

analytical estimate $\arctan(\sqrt{R^{\mathrm{bc}}_{\mathrm{ow}}})$*, in the first and second layer respectively in regions of large total-energy extraction. The dashed lines in Figs. 2(a) and (b) suggest, as already noted previously, that the perturbation in the first layer extracts energy from the basic flow much more barotropically than baroclinically and that the opposite seems to occur in the second layer. This intuitive result inferred from the PDFs of $\varphi' - \pi/2$ is clearly confirmed by Figs. 4(a) and (c). Indeed, in the first layer (Fig. 4(a)), most of the points are close to $(\pi/2, \pi/2)$ which means that R^{bc} (as well as $R^{\mathrm{bc}}_{\mathrm{ow}}$) is large, whereas in Fig. 4(c) most of the points are close to $(0, 0)$, which means that R^{bc} (as well as $R^{\mathrm{bc}}_{\mathrm{ow}}$) is small in the second layer. Another result is that the first bisecting line is clearly the privileged axis in the two figures; it shows that $R^{\mathrm{bc}}_{\mathrm{ow}}$, the ratio estimated by using the productive eigenvector of $\overline{\mathbf{A}}$, whose expression is given in terms of the basic-state terms in Eq. (30), is a good diagnostic of the actual ratio R^{bc} at each grid point in each layer. A simpler rough analytical diagnostic of R^{bc} could have been the ratio of the rate of strain $\overline{\sigma} = max(\delta^{\mathrm{b}})$ to the vertical shear $\overline{\sigma}_z = max(\delta^{\mathrm{c}})$. The joint PDFs of $\arctan(\sqrt{|R^{\mathrm{bc}}|})$ with $\arctan(\sqrt{\overline{\sigma}/\overline{\sigma}_z})$ in the first and second layer (Figs. 4(b) and (d)) show that most of the points do not lie close to the first bisecting line. An interesting result of the two previous joint PDFs is that the rough estimate, $\arctan(\sqrt{\overline{\sigma}/\overline{\sigma}_z})$, underestimates the difference between the two generation rates. Indeed, in the first layer where the barotropic generation rate is significantly greater than the baroclinic one, R^{bc} is greater than $\overline{\sigma}/\overline{\sigma}_z$ ($|R^{\mathrm{bc}}| \simeq R^{\mathrm{bc}}_{\mathrm{ow}} \gg \overline{\sigma}/\overline{\sigma}_z \gg 1$), whereas in the second layer where the reverse occurs, R^{bc} is smaller than $\overline{\sigma}/\overline{\sigma}_z$ ($|R^{\mathrm{bc}}| \simeq R^{\mathrm{bc}}_{\mathrm{ow}} \ll \overline{\sigma}/\overline{\sigma}_z \ll 1$). The main conclusion of this paragraph is that our analytical expression $R^{\mathrm{bc}}_{\mathrm{ow}}$ (see Eq. (30)) is quite relevant for diagnosing the ratio R^{bc} whereas the rougher estimate $\overline{\sigma}/\overline{\sigma}_z$ is not. $R^{\mathrm{bc}}_{\mathrm{ow}}$ can therefore be useful for identifying regions where barotropic or baroclinic processes prevail for a given flow.

(iv) *Comparison with the Eady index.* The Eady index is used in numerous papers (e.g. Hoskins and Valdes 1990; Buizza and Palmer 1995) to localize regions of strong baroclinicity

$$\sigma_{\mathrm{Eady}} = 0.31 \frac{f}{N} \left| \frac{\partial \overline{\mathbf{u}}}{\partial z} \right| = 0.31 \, \overline{\sigma}_z, \tag{33}$$

and corresponds to the largest growth rate of the unstable normal mode in the Eady model. The Eady index can be viewed as the multiplication of the maximum of δ^{c}, i.e. $\overline{\sigma}_z$, by 0.31. The purpose of the present paragraph is to show that our analytical expression $\delta^{\mathrm{c}}_{\mathrm{ow}}$ is more relevant than the Eady parameter as an estimate at each grid point of the Monte-Carlo baroclinic generation rate, $\delta^{\mathrm{c}}_{\mathrm{MC}}$. A joint PDF of $\delta^{\mathrm{c}}_{\mathrm{MC}}$ with the Eady parameter in regions of large baroclinic extraction shows a cloud of points that are rather scattered whereas a joint PDF of $\delta^{\mathrm{c}}_{\mathrm{MC}}$ with our analytical estimate $\delta^{\mathrm{c}}_{\mathrm{ow}}$ is centred around the first bisecting line (see Fig. 5). In other words, at each grid point, the vertical slope of the perturbation isolines results from the complex local interaction between the horizontal deformation and the vertical shear and is not, of course, simply the vertical slope corresponding to the unstable normal mode of the Eady model. Our analytical expression $\delta^{\mathrm{c}}_{\mathrm{ow}}$ is much more accurate at each grid point for diagnosing the real generation rate $\delta^{\mathrm{c}}_{\mathrm{MC}}$ than the Eady parameter, and should be a new relevant parameter for diagnosing regions of strong baroclinic activity.

---

* The use of the operator $\arctan(\sqrt{.})$ allows us to recover a quantity homogeneous to the angle $\varphi'^{\mathrm{row}}_{-}$ following Eq. (30).
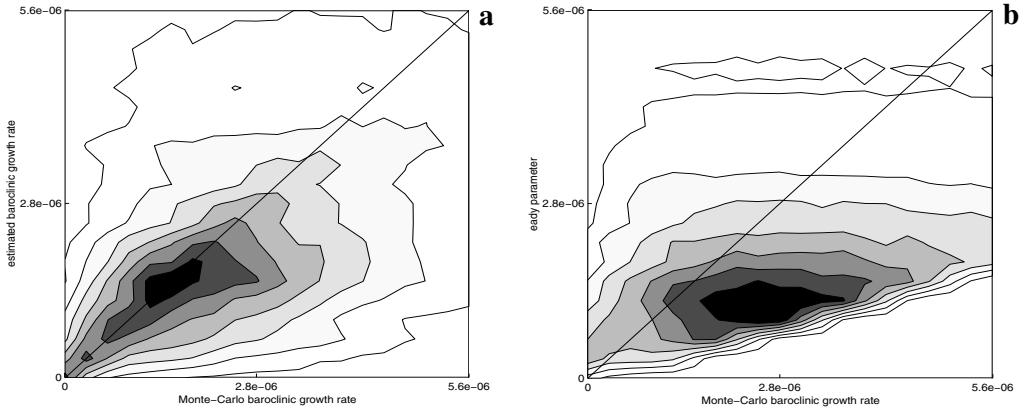
Figure 5.　Joint probability density functions at $T = 20$ days in the second layer of the Monte-Carlo baroclinic generation rate with (a) the analytical estimate, δ^c_{ow}, and (b) the Eady index in the same regions as in Fig. 4 (see text for details).

(v)　*Check on the consistency of the approximation of the ageostrophic terms.* The analytical expressions for the baroclinic ageostrophic vector $\mathbf{v}_{\chi,w}$ and the barotropic ageostrophic vector $\mathbf{v}_p$ show that the two vectors align respectively with $\mathbf{e}'_{3\perp}$ and $\mathbf{e}'_{\perp}$. This is usually not true in our numerical simulations, and their projection onto $\mathbf{e}'_3$ is not trivial as they correspond to the essential redistribution processes of energy as shown by Cai and Mak (1990). However, we have verified numerically that there is a tendency for the two ageostrophic vectors to be closer respectively to the directions of $\mathbf{e}'_{3\perp}$ and $\mathbf{e}'_{\perp}$ than to the other vectors. The analytical predictions are roughly confirmed in the numerical results, even if projections onto $\mathbf{e}'_3$ are found to be important for the redistribution processes.

　　Furthermore, we have drawn the joint PDF of $(\mathbf{v}_{\chi,w} \cdot \mathbf{e}'_{3\perp})/|\mathbf{u}'_3|$ (not shown here) with the analytical approximation of Eq. (24); most of the points are clustered around the point (0,0). This means that for the eigenvectors' directions, the baroclinic ageostrophic vector is close to zero, which confirms our analytical prediction. The cloud of points obtained with this joint PDF forms an ellipsoid (similar to Fig. 8 of RHK), whose principal axis is not too far from the first bisecting line. This numerical result shows that the analytical approximation is significant and that the baroclinic ageostrophic vector acts in such a way that $\varphi^{row}_{\pm}$ are still the preferred directions of the complete equation of φ'. This result is equivalent to the result shown in Fig. 8 of RHK for the diagnostic of the ageostrophic pressure effect. The analytical approximations provide a rationale for the main role of the ageostrophic terms and explains why the eigenvector structures of $\overline{\mathbf{A}}$ are the most probable perturbation structures in QG flows since their directions correspond to the preferred directions by considering the complete system (Eq. (4)).

(b)　*Finite time error fields*

　　The alignment analysis of the previous section has shown that, with the knowledge of the basic-state structure, we can predict the most probable angle φ' and thus the most probable ratio of the perturbation kinetic energy over its potential energy at each grid point. However the finite time error fields per se, for the perturbation kinetic energy (potential energy or total energy) K' (P' or $|\mathbf{u}'_3|^2/2$), cannot be deduced from our instantaneous local methodology which does not take into account the past history of
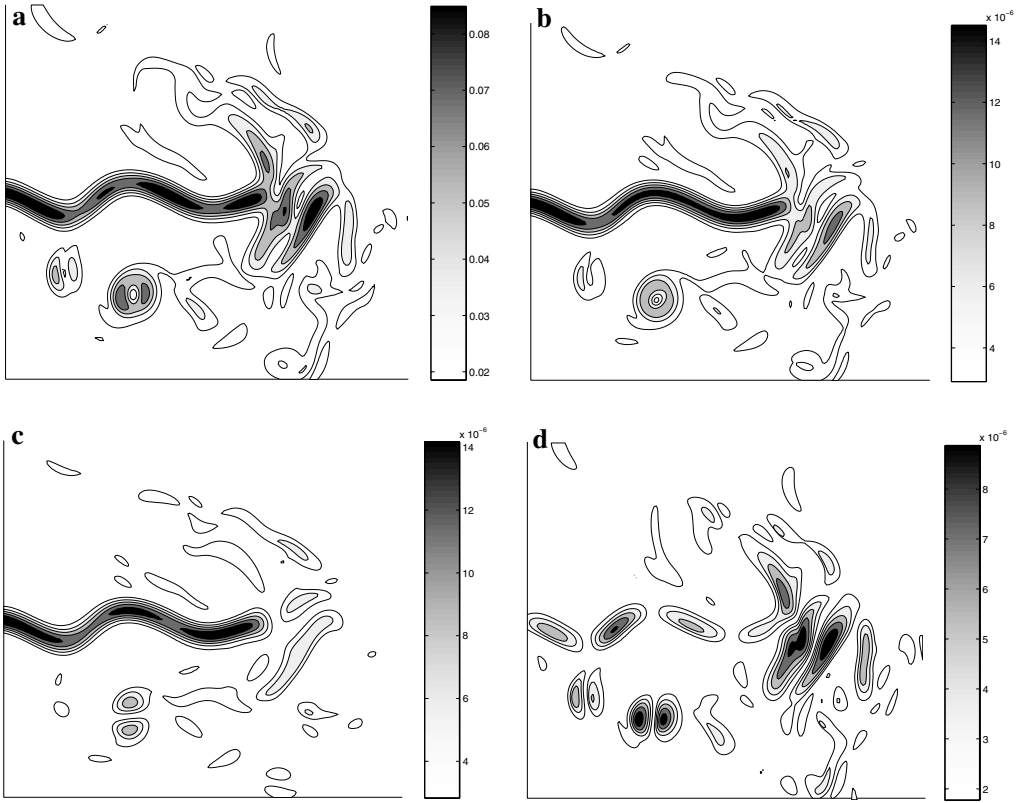
Figure 6. Comparison between spatial structures of the potential-energy error field, $|\partial_z \psi'|/\sqrt{S}$, and spatial properties of the basic-state vertical-shear strain rate, $\overline{\sigma}_z$, in the first layer; (a) r.m.s. of the potential-energy error field , (b) vertical-shear strain rate, $\overline{\sigma}_z$, (c) vertical zonal-shear strain rate, $|\partial_z \overline{u}|/\sqrt{S}$, and (d) vertical meridional-shear strain rate, $|\partial_z \overline{v}|/\sqrt{S}$. Units for (a) are m s^{-1}, and for (b), (c) and (d) are s^{-1}.

the perturbations. Nevertheless results in RHK concerning the kinetic-energy error field K' show that maxima of K' are localized in specific regions, where the norm of $\nabla \overline{\mathbf{u}}$ is large. Similarly error maxima in PV are localized in regions of large PV gradient of the reference flow. This interesting result can also be generalized for the potential-energy and the total-energy fields, as we will see below.

Let us first focus on potential energy. The r.m.s. of P', again calculated with 200 perturbations, is plotted in an area located at the end part of the jet after 20 days in Fig. 6(a). We compare the r.m.s. of P' (Fig. 6(a)) with $|\partial_z \overline{u}|/\sqrt{S}$ (Fig. 6(c)), $|\partial_z \overline{v}|/\sqrt{S}$ (Fig. 6(d)) and $\overline{\sigma}_z = \sqrt{(\partial_z \overline{u})^2 + (\partial_z \overline{v})^2}/\sqrt{S}$ (Fig. 6(b)). It is clear that the details of the local structures of P' are very well represented by $\overline{\sigma}_z$ and not completely by $|\partial_z \overline{u}|/\sqrt{S}$ alone or by $|\partial_z \overline{v}|/\sqrt{S}$ alone; the correlations between the r.m.s. of P' and $\overline{\sigma}_z$, $|\partial_z \overline{u}|/\sqrt{S}$ and $|\partial_z \overline{v}|/\sqrt{S}$ are 0.98, 0.85 and 0.84, respectively. As errors in PV are localized in regions of strong basic-state PV gradient (see RHK) and errors in potential energy are localized in regions of large values of $\overline{\sigma}_z$, a generic property seems to emerge. For a given geostrophic scalar variable $\overline{s}$ (e.g. all spatial derivatives of the geostrophic stream function), whose time evolution is described by an equation such as $\overline{D\overline{s}}/Dt = \textit{ageostrophic terms}$, the error field associated with this variable, s', is

localized in regions of large $|\nabla \bar{s}|$. This characteristic is suggested by the linearization of the previous equation, $\overline{D}s'/Dt = -\mathbf{u}' \cdot \nabla \bar{s} + \textit{perturbation ageostrophic terms}$, in which $\nabla \bar{s}$ appears.

In RHK, maxima of K' are shown to be localized in regions where the norm of $\nabla \overline{\mathbf{u}}$ is large. In the same manner, by drawing a parallel between Eqs. (1) and (4), maxima of total energy should be localized in regions where the norm of $\overline{\mathbf{A}}$ is large. This intuitive result was confirmed by our numerical results (not shown here).

4.   CONCLUSION

We can summarize the main results of the paper as follows. The most probable 3D perturbation structure in QG flows is analytically given at each time by the two non-trivial eigenvectors of the 3D basic-state velocity gradient tensor, $\overline{\mathbf{A}}$, in specific regions where the strain rate is larger than the relative vorticity ($|r_{\mathrm{ow}}| < 1$). This result was first diagnosed by analysing analytically the linearized perturbation equations and the ageostrophic terms, and has been confirmed by numerical results using Monte-Carlo techniques. The eigenvector structure inducing perturbation growth enables us to diagnose the most probable total-energy generation rate in regions where $|r_{\mathrm{ow}}| < 1$. The total generation rate of the productive eigenvector is decomposed into the sum of a positive barotropic generation rate and a positive baroclinic generation rate. The productive eigenvector is also useful to give an approximation of the ratio of the perturbation kinetic energy over its potential energy at each grid point, as well as a diagnostic of the ratio of the barotropic conversion term to the baroclinic one.

Section 2(e) showed that the preferential orientation leading to perturbation growth is generally distinct from the strain contraction axis, i.e. from the singular vectors optimizing short times. The preferential orientations that emerge after a finite time can be viewed as a rationalization of the Lagrangian equilibrium properties of the perturbations that have grown in the past, and as such are closer to bred vectors or backward Lyapunov vectors. The latter point is elaborated in detail in Rivière and Hua (2004).

An intercomparison between the Eady index and our analytical diagnostic of the exponential baroclinic generation rate, $\delta_{\mathrm{ow}}^{\mathrm{c}}$, has shown that our analytical diagnostic derived from the productive eigenvector of $\overline{\mathbf{A}}$ is more relevant than the Eady index to estimate at each grid point the value of the Monte-Carlo exponential baroclinic generation rate, δ^{c}.

Concerning the relevance of the regions where $|r_{\mathrm{ow}}| < 1$ in the topology of the perturbation, these regions represent two thirds of the regions of large exponential barotropic generation rate and around 60% of the regions of large exponential baroclinic generation rate. Regions where $|r_{\mathrm{ow}}| > 1$ are therefore less relevant to perturbation energy extraction, even if their dynamics are not negligible. Further studies are needed to detect the preferential perturbation structure in the latter regions.

The spatial localization of the error fields can be diagnosed quite well by analytical diagnostics even if we cannot explain these relations by our approach. Indeed, our Lagrangian approach gives information about the perturbation structures and the generation rates, but as it cannot give information about the redistribution processes, we cannot explain the local Eulerian growth rate. The spatial relations between the error fields and their corresponding basic-state fields are however strong. For example, the maxima of the total-energy error field are localized in regions where the norm of $\overline{\mathbf{A}}$ is large and those of the potential-energy error field in regions where the vertical strain rate is the largest.

REFERENCES

Bishop, C. H.	1993	On the behaviour of baroclinic waves undergoing horizontal deformation. I: The 'RT' phase diagram. *Q. J. R. Meteorol. Soc.*, **119,** 221–240
Bishop, C. H. and Thorpe, A. J.	1994	Frontal wave stability during moist deformation frontogenesis. Part I: Linear wave dynamics. *J. Atmos. Sci.*, **51,** 852–873
Buizza, R. and Palmer, T. N.	1995	The singular vector structure of the atmospheric global circulation. *J. Atmos. Sci.*, **52,** 1434–1456
Cai, M. and Mak, M.	1990	On the basic dynamics of regional cyclogenesis. *J. Atmos. Sci.*, **47,** 1417–1442
Charney, J. G.	1947	The dynamics of long waves in a baroclinic westerly current. *J. Meteorol.*, **4,** 135–163
Craik, A. D. D. and Criminale, W. O.	1986	Evolution of wavelike disturbances in shear flows: a class of exact solutions of the Navier-Stokes equations. *Proc. R. Soc. London,* **A406,** 13–26
Eady, E. T.	1949	Long waves and cyclone waves. *Tellus*, **1,** 33–52
Farrell, B. F.	1982	The initial growth of disturbances in a baroclinic flow. *J. Atmos. Sci.*, **39,** 1663–1686
	1989	Transient development in confluent and diffluent flow. *J. Atmos. Sci.*, **46,** 3279–3288
Farrell, B. F. and Ioannou P. J.	1996	Generalized stability theory. part I: autonomous operators. *J.Atmos. Sci.*, **53,** 2025–2040
Frederiksen, J. S.	2000	Singular vectors, finite-time normal modes, and error growth during blocking. *J. Atmos. Sci.*, **57,** 312–333
Haynes, P. and Anglade, J.	1997	The vertical-scale cascade in atmospheric tracers due to large-scale differential advection. *J. Atmos. Sci.*, **54,** 1121–1136
Hoskins, B. J., Draghici, I. and Davies, H. C.	1978	A new look at the ω-equation. *Q. J. R. Meteorol. Soc.*, **104,** 31–38
Hoskins, B. J. and Valdes, P. J.	1990	On the existence of storm tracks. *J. Atmos. Sci.*, **47,** 1854–1864
Hua, B. L., McWilliams, J. C. and Klein, P.	1998	Lagrangian accelerations in geostrophic turbulence. *J. Fluid Mech.*, **366,** 87–108
Iacono, R.	2002	Local energy generation in barotropic flows. *J. Atmos. Sci.*, **59,** 2153–2163
James, I. N.	1987	Suppression of baroclinic instability in horizontally sheared flows. *J. Atmos. Sci.*, **44,** 3710–3720
Lapeyre, G., Klein, P. and Hua, B. L.	1999	Does the tracer gradient vector align with the strain eigenvectors in 2D turbulence? *Phys. Fluids A*, **11,** 3729–3737
Mak, M. and Cai, M.	1989	Local barotropic instability. *J. Atmos. Sci.*, **46,** 3289–3311
Orr, W. M.	1907	Stability or instability of the steady motions of a perfect liquid. *Proc. R. Irish Acad.*, **27,** 9–69
Rivière, G. and Hua, B. L.	2004	An analytical approach for diagnosing areas of strong error growth in quasigeostrophic flows. *Tellus*, in press
Rivière, G., Hua, B. L. and Klein, P.	2003	Perturbation growth in terms of barotropic alignment properties. *Q. J. R. Meteorol. Soc.*, **129,** 2613–2635
Simmons, A. J. and Hoskins, B. J.	1980	Barotropic influences on the growth and decay of baroclinic waves. *J. Atmos. Sci.*, **37,** 1679–1684
Snyder, C. and Joly, A.	1998	Development of perturbations within a growing baroclinic wave. *Q. J. R. Meteorol. Soc.*, **124,** 1961–1983
Szunyogh, I., Kalnay, E. and Toth, Z.	1997	A comparison of Lyapunov and singular vectors in a low resolution GCM. *Tellus*, **49A,** 200–227